CHALMERS
UNIVERSITY OF TECHNOLOGY

Low-Threshold AlGaN-based UVB VCSELs enabled by post-growth cavity detuning

Applied Physics Letters

Low-threshold AlGaN-based UVB VCSELs enabled by post-growth cavity detuning

Cite as: Appl. Phys. Lett. **121**, 103501 (2022); https://doi.org/10.1063/5.0097903
Submitted: 03 May 2022 • Accepted: 17 August 2022 • Published Online: 07 September 2022

G. Cardinali, F. Hjort, N. Prokop, et al.

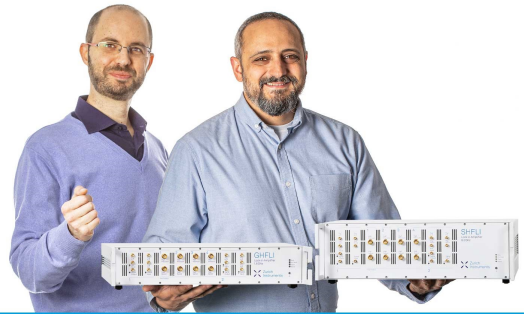

Applied Physics Letters ARTICLE scitation.org/journal/apl

Low-threshold AlGaN-based UVB VCSELs enabled by post-growth cavity detuning

Cite as: Appl. Phys. Lett. **121**, 103501 (2022); doi: 10.1063/5.0097903
Submitted: 3 May 2022 · Accepted: 17 August 2022 ·
Published Online: 7 September 2022

G. Cardinali,[1] F. Hjort,[2] N. Prokop,[1] J. Enslin,[1] M. Cobet,[1] M. A. Bergmann,[2] J. Gustavsson,[2] J. Ciers,[2] I. Häusler,[3] T. Kolbe,[4] T. Wernicke,[1] Å. Haglund,[2,a)] and M. Kneissl[1,4]

AFFILIATIONS

[1]Institute of Solid State Physics, Technische Universität Berlin, Hardenbergstraße 36, 10623 Berlin, Germany
[2]Department of Microtechnology and Nanoscience, Chalmers University of Technology, 41296 Gothenburg, Sweden
[3]Institute of Optics and Atomic Physics, Technische Universität Berlin, Hardenbergstraße 36, 10623 Berlin, Germany
[4]Ferdinand-Braun-Institut (FBH), Gustav-Kirchhoff-Str. 4, 12489 Berlin, Germany

[a)]Author to whom correspondence should be addressed: asa.haglund@chalmers.se

ABSTRACT

The performance of vertical-cavity surface-emitting lasers (VCSELs) is strongly dependent on the spectral detuning between the gain peak and the resonance wavelength. Here, we use angle-resolved photoluminescence spectroscopy to investigate the emission properties of AlGaN-based VCSELs emitting in the ultraviolet-B spectral range with different detuning between the photoluminescence peak of the quantum-wells and the resonance wavelength. Accurate setting of the cavity length, and thereby the resonance wavelength, is accomplished by using doping-selective electrochemical etching of AlGaN sacrificial layers for substrate removal combined with deposition of dielectric spacer layers. By matching the resonance wavelength to the quantum-wells photoluminescence peak, a threshold power density of 0.4 MW/cm^2 was achieved, and this was possible only for smooth etched surfaces with a root mean square roughness below 2 nm. These results demonstrate the importance of accurate cavity length control and surface smoothness to achieve low-threshold AlGaN-based ultraviolet VCSELs.

Vertical-cavity surface-emitting lasers (VCSELs) have many advantageous properties including single longitudinal mode emission, circular and low-divergent output beams, low threshold currents, and the possibility of integration in 2D arrays.[1] Due to these characteristics, AlGaN-based ultraviolet (UV) VCSELs could enable a broad range of applications, such as phototherapy,[2,3] gas sensing,[4] UV curing,[5] high-resolution printing,[6] and disinfection.[7–9] Recently, the first optically pumped ultraviolet-B (UVB, 280–320 nm)[10] and ultraviolet-C (UVC, <280 nm)[11] VCSELs were demonstrated raising the hope for a swift development of the field of surface-emitting UV lasers.[12] However, limited cavity length control impairs the performance of these devices, resulting in high thresholds and multimode emission.

The VCSEL's static and dynamic performance characteristics strongly depend on the spectral separation between the resonance wavelength, which is set by the cavity length and the quantum-wells gain peak (i.e., detuning). The gain spectrum and the resonance wavelength redshift with increasing temperature,[13–15] but at different rates. Moreover, the gain spectrum of InGaN[16] and AlGaN[17] quantum-wells (QWs) blueshifts with increasing carrier concentration. Therefore, the spectral overlap between the relatively broad gain spectrum and the narrow resonance peak changes with operating conditions. Lasing is only possible if the gain at the resonance wavelength is high enough to compensate for the losses. Depending on the internal losses, the confinement factor of the optical mode, and the shift of the gain spectrum with carrier density, an optimal detuning can be determined to achieve the lowest threshold.[18]

The detuning can be adjusted by controlling the thickness of the epitaxially grown cavity layers, which puts stringent requirements on the growth process. Post-growth thickness adjustment can be implemented by adding a dielectric spacer between the cavity and the dielectric mirror. In GaN-based VCSELs, such dielectric layer is used between the ITO and the p-side distributed Bragg reflector (DBR) to place the highly absorbing ITO-layer in an optical standing field minimum.[13,19–24] Ideally, a spacer should be deposited on both sides of the cavity before the DBRs deposition to align the standing optical field distribution with the loss and gain regions. This requires a substrate removal technique that can provide reproducible and homogeneous device thicknesses and smooth interfaces. Post-growth cavity length

adjustment can especially be important for electrically injected UV VCSELs, which will likely need tunnel junctions (TJs). These TJs have a high optical absorption and, therefore, need to be placed exactly at a node of the optical field, as seen in blue VCSELs.[25–27]

The most common substrate removal techniques implemented for GaN-based VCSELs are laser liftoff and chemical mechanical polishing.[13,28–30] However, applying such methods to AlGaN can lead to rough surfaces, formation of cracks in the epitaxial layers, or poor thickness control.[31–33] Photoelectrochemical etching (ECE) has also been used in violet and blue VCSELs;[15,34] however, it requires homogeneous illumination of the device and specific design of the epitaxial structure.[35–37] An alternative substrate removal technique is doping-selective electrochemical etching (ECE) of AlGaN, which has been recently demonstrated by our groups[36] and applied for the fabrication of thin-film UVB LEDs[37] and VCSELs,[10] allowing for the fabrication of AlGaN membranes with smooth surfaces and controlled thickness.

In this work, the emission properties of optically pumped UVB VCSELs with different detuning and cavity surface roughness are investigated. The detuning is varied by depositing dielectric spacers after substrate removal by electrochemical etching. These results demonstrate the importance of precise cavity length control and surfaces smoothness for the development of low-threshold UV VCSELs.

Figure 1(a) shows a schematic of the VCSELs epitaxial structures, grown by metal-organic vapor phase epitaxy (MOVPE) pseudomorphically strained to AlGaN pseudosubstrates.[38] The structures consist of a current spreading layer for the ECE with Si concentration of $2 \times 10^{18}\,\mathrm{cm}^{-3}$, an etch stop layer with Si concentration of $0.5 \times 10^{18}\,\mathrm{cm}^{-3}$, and a sacrificial layer with Si concentration of $2 \times 10^{19}\,\mathrm{cm}^{-3}$, followed by an unintentionally doped 2.5λ $Al_{0.6}Ga_{0.4}N$ cavity containing $Al_{0.5}Ga_{0.5}N/Al_{0.2}Ga_{0.8}N$ quantum wells (QWs). More details on epitaxial growth and VCSEL fabrication can be found in Ref. 10. Two structures were grown: epitaxy A with five QWs and a 130-nm-thick $Al_{0.22}Ga_{0.78}N$ bulk sacrificial layer, and epitaxy B with three QWs and a sacrificial multilayer having a 100-nm-thick $Al_{0.39}Ga_{0.61}N$ layer with five periods of an $Al_{0.11}Ga_{0.89}N/Al_{0.39}Ga_{0.61}N$ 5/5 nm short-period superlattice (SPSL) on top. Figure 1(b) shows the emission spectra, integrated over the emission angles, of the as-grown epitaxial structures at an excitation power density of $1\,\mathrm{MW/cm}^2$. The photoluminescence (PL) measurements were performed in an angle resolved PL setup with a diode-pumped solid-state frequency-quadrupled Nd:YAG excitation laser emitting at 266 nm with a repetition rate of 60 Hz and a pulse width of 1.3 ns, providing an excitation spot diameter of 10 μm. Epitaxy A shows a peak emission of 318.2 nm with a variation of ± 1 nm across a $5 \times 5\,\mathrm{mm}^2$ area, attributed to compositional and thickness fluctuations within the QWs. Epitaxy B shows a homogeneous emission around 317.2 nm with ± 0.3 nm of variation across an area with similar dimensions as above.

In the VCSELs fabrication, device mesas were etched and covered with an 11-pair HfO_2/SiO_2 DBR with respective layer thicknesses of 36.2 and 53.8 nm, an Al mirror, a SiO_2 layer, and Ti/Au bonding metals. The devices were underetched using ECE at 30 V in 0.3 M HNO_3, as described in Ref. 10, and then bonded to an Au-covered Si carrier. As shown in Figs. 1(c) and 1(d), the electrochemically etched surface of epitaxy A had a root mean square (RMS) roughness of 3.9 nm over a $5 \times 5\,\mu\mathrm{m}^2$ area, while the preferential etching at the top of the sacrificial multilayer in epitaxy B resulted in a smoother surface with an RMS roughness of 1.7 nm (similar to the 2.2 nm RMS of the as-grown epitaxy). Here, the built-in polarization fields in the multilayer enhances the etch selectivity and causes an abrupt stop of the etching process, resulting in a smoother surface.[39] After flip-chip bonding, the devices were finalized by depositing a top 10-pair HfO_2/SiO_2 DBR. A fully processed VCSEL is shown schematically in Fig. 1(e) and in a cross-sectional transmission electron microscopy (TEM) image in Fig. 1(f).

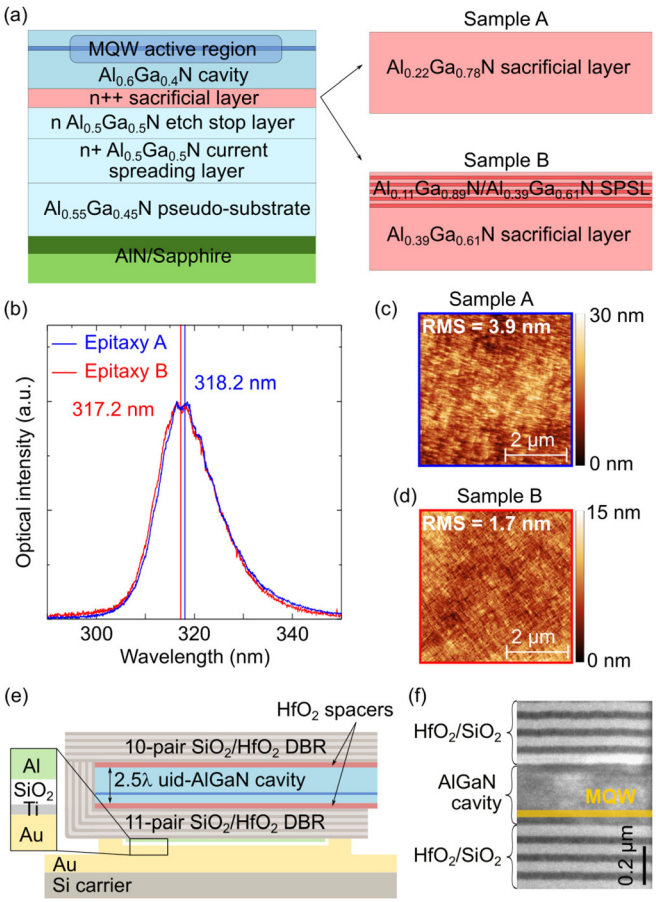

FIG. 1. (a) Schematic of the as-grown epitaxy with details on the two different sacrificial layers used. (b) Photoluminescence spectrum of the as-grown epitaxy A and B at an excitation power density of $1\,\mathrm{MW/cm}^2$. (c) Atomic force microscopy image of the N-polar AlGaN cavity surface exposed by electrochemically etching a bulk and (d) a multilayered sacrificial layer. (e) Schematic of the UVB VCSEL structure with HfO_2 spacers above and below the AlGaN cavity. (f) Transmission electron microscopy image of a VCSEL cavity without HfO_2 spacers released by electrochemically etching the sacrificial multilayer.

To investigate the impact of the detuning on the VCSELs performance, devices with shifted resonance wavelengths were fabricated by adding HfO_2 spacers between the AlGaN cavity and the DBRs. Six VCSELs samples were fabricated, three using epitaxy A grown with the bulk sacrificial layer and three using epitaxy B grown with the sacrificial multilayer. The samples from epitaxy A were a cavity defined by the as-grown epitaxy (VCSELs A0); a sample targeting a resonance shift of +5 nm (VCSELs A + 5) and, therefore, a 7.3 nm HfO_2 spacer on the N-polar cavity surface and 3.1 nm on the metal-polar cavity surface; and a sample targeting a shift of -5 nm (VCSELs A−5) and,

therefore, with reduced first SiO_2 layer in the DBRs. Epitaxy B had a thinner $Al_{0.6}Ga_{0.4}N$ layer on the N-polar cavity side than targeted (a total cavity thickness of 327 nm for epitaxy A and 310 nm for epitaxy B was determined by *in situ* measurements during growth). Therefore, a HfO_2 spacer was only deposited on the N-polar cavity surface. The samples fabricated from epitaxy B were a cavity defined by the as-grown epitaxy (VCSELs B0); a sample targeting a shift of +5 nm (VCSELs B + 5) and, therefore, a 10.4-nm-thick HfO_2 spacer; and a sample targeting a shift of +13 nm (VCSELs B + 13) and, therefore, a 27-nm-thick HfO_2 spacer.

The optical pumping experiments were performed in the same angle resolved PL setup described before. The emission from the VCSELs was collected through a microscope objective with a numerical aperture of 0.4, corresponding to a collection angle of ±24°. The angular resolved far-field was obtained by using a 4f-geometry to image the Fourier plane on the monochromator entrance slit.[40] More information about this can be found in the supplement of Ref. 10. The wave vector distribution in a VCSEL is directly proportional to the emission angle of the far field; therefore, using angular-resolved PL, it is possible to distinguish between the non-dispersive unfiltered emission and the parabolically dispersed longitudinal cavity mode.[41] This allows for quantifying the detuning and investigating its impact on the laser characteristics.

In the following, the impact of the detuning on the threshold power density will be discussed for the VCSELs grown on the multilayered sacrificial layer with shifted resonance wavelength. These results will be then compared to measurements on VCSELs grown on the bulk sacrificial layer with larger cavity surface roughness, to investigate the influence of the surface smoothness on the emission characteristic of UVB VCSELs. Figure 2(a) shows the calculated resonance wavelength of a 2.5λ cavity as a function of the cavity length deviation using a 1D scalar wave effective index method.[42] The resonance wavelength shifts linearly with the cavity length, where a 1 nm thickness deviation results in a 0.55 nm spectral shift. The addition of HfO_2 layers will serve as an extension of the cavity, since the refractive index

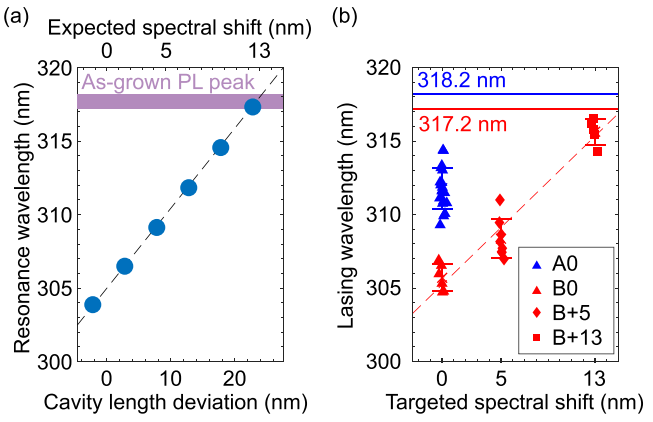

FIG. 2. (a) Calculated resonance wavelength of the 2.5λ longitudinal cavity mode as a function of the thickness deviation of the $Al_{0.6}Ga_{0.4}N$ cavity. (b) Measured lasing wavelengths as a function of the targeted spectral shift for VCSELs with cavity released by etching different sacrificial layers. The red dashed line is a guide to the eye, and the horizontal continuous lines indicate the as-grown PL peak of epitaxy A (blue) and B (red).

difference between $Al_{0.6}Ga_{0.4}N$ and HfO_2 is less than 10% and no subcavity is thereby formed by the HfO_2 layer. Figure 2(b) shows the measured lasing wavelengths of VCSELs with different HfO_2-spacer thicknesses. As most of the samples showed multimode-emission, the lasing wavelength is defined as the wavelength of the lasing peak with the highest intensity at 1.5 times the threshold of the first appearing mode. The processed VCSELs from epitaxy B show a linear increase in the lasing wavelength with increasing targeted spectral shift, matching the trend predicted by the simulations. The variation in lasing wavelength for devices on the same sample is associated with lateral sample inhomogeneities.[10] The VCSELs processed using epitaxy A with the bulk sacrificial layer only lased for a zero targeted spectral shift (explained in more detail later), showing a longer lasing wavelength compared to the VCSELs from epitaxy B without spacers due to the different thickness of the as-grown AlGaN cavity.

Figure 3 shows angle-resolved PL spectra below and above threshold of VCSELs B + 5 and B + 13 grown with the sacrificial multilayer. For the VCSEL B + 5 [Fig. 3(a)], the broad non-dispersive light emitted from the QWs matches the as-grown PL peak, indicated by the vertical red line at 317.2 nm. A portion of this spontaneous emission is coupled into the parabolically dispersed 2.5λ cavity mode visible between 305 and 310 nm. Above threshold, multiple lasing peaks arise and the sharp transition to lasing is confirmed by beam and linewidth narrowing. The brightest lasing line emerges at 309.4 nm in correspondence to the minimum of the cavity mode dispersion at k = 0, yielding a detuning of +7.8 nm. The detuning will here be defined as the as-grown PL peak wavelength measured at 1 MW/cm^2 [see Fig. 1(b)] minus the lasing wavelength, as commonly done for VCSELs. In the VCSEL B + 13 [Fig. 3(b)], the non-dispersive emission is not visible, indicating a stronger coupling of the QWs into the cavity resonance. Above threshold, a lasing peak arises at 316.2 nm yielding a detuning of +1 nm. These results show the effectiveness of shifting the resonance wavelength by adding a dielectric spacer.

Figure 4(a) shows the emission spectra at different pump power densities of the VCSEL B + 5. A single mode is dominant below 1.3 times the threshold power density, while multimode emission becomes dominant at higher pump power densities. Similar behavior was observed in the majority of the samples and the strong multi-peak characteristic is attributed to filamentary lasing,[10] widely observed in III-nitride VCSELs.[21,43,44] For the VCSEL B + 13 [Fig. 4(b)], the main lasing peak arises at 316.2 nm and is maintained dominant up to 1.2 MW/cm^2, with a secondary peak at 316.4 nm. Figure 4(c) shows a high-resolution spectrum above threshold measured in another setup using a 266 nm pump laser with 20.5 kHz repetition rate, 0.55 ns pulse width, and a 3 μm pump spot diameter, showing a full width at half maximum of 0.03 nm. Figure 4(d) shows the integrated emission intensity around the dominant lasing peak as a function of the pump power density for VCSELs fabricated from epitaxy B with the sacrificial multilayer. A threshold power density of 0.7 MW/cm^2 is achieved for a VCSEL with +1 nm detuning, while the threshold increases more than one order of magnitude for devices with large detuning, demonstrating the importance of controlling the cavity length on a nm-scale in VCSELs.

In order to study the effect of the surface roughness on the VCSEL's lasing performance, the previously reported results for VCSELs B (sacrificial multilayer) are compared to the measurements on VCSELs A (bulk sacrificial layer), exhibiting a larger N-polar cavity

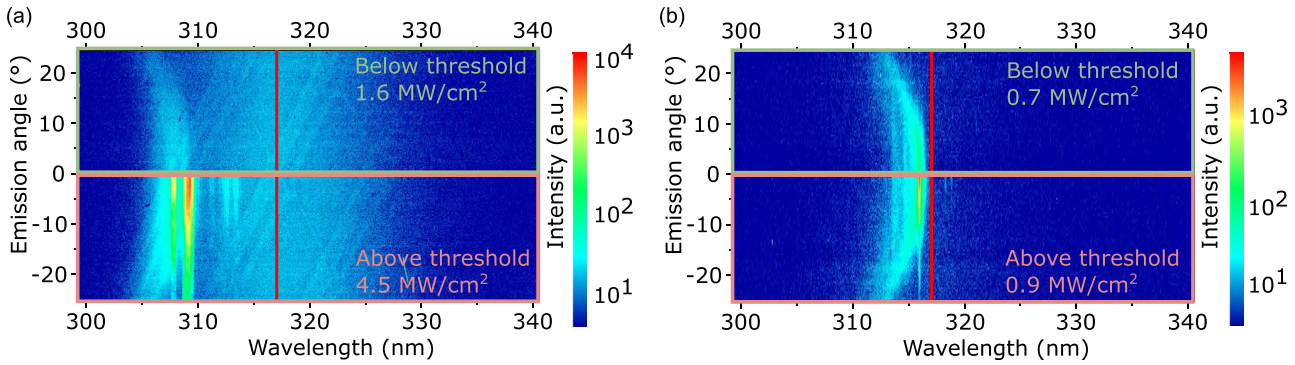

FIG. 3. Angle-resolved PL spectra below and above threshold for VCSELs (a) B + 5 with +7.8 nm detuning and (b) B + 13 with +1 nm detuning. The vertical red line at 317.2 nm indicates the as-grown PL peak of epitaxy B.

surface RMS roughness of 3.9 nm compared to the 1.7 nm RMS roughness measured for the VCSELs with cavity released by etching the sacrificial multilayer [see Figs. 1(c) and 1(d)]. Figure 5 shows the threshold power densities as a function of the detuning for all investigated VCSELs. The VCSELs fabricated from epitaxy B (sacrificial multilayer) show a reduction of the threshold power density from 10.8 MW/cm^2 for VCSELs B0 without spacers to 0.6 MW/cm^2 for VCSELs B + 13 with +13 nm targeted spectral shift, on average. The lowest threshold power density of 0.4 MW/cm^2 was achieved for a VCSEL B + 13 with a detuning of +0.7 nm. In the case of the processed VCSELs from epitaxy A (bulk sacrificial layer), lasing was achieved only for the sample without HfO_2 spacers, exhibiting a detuning between 4 and 9 nm. The threshold power density for this sample was on average higher than for devices with cavity underetched

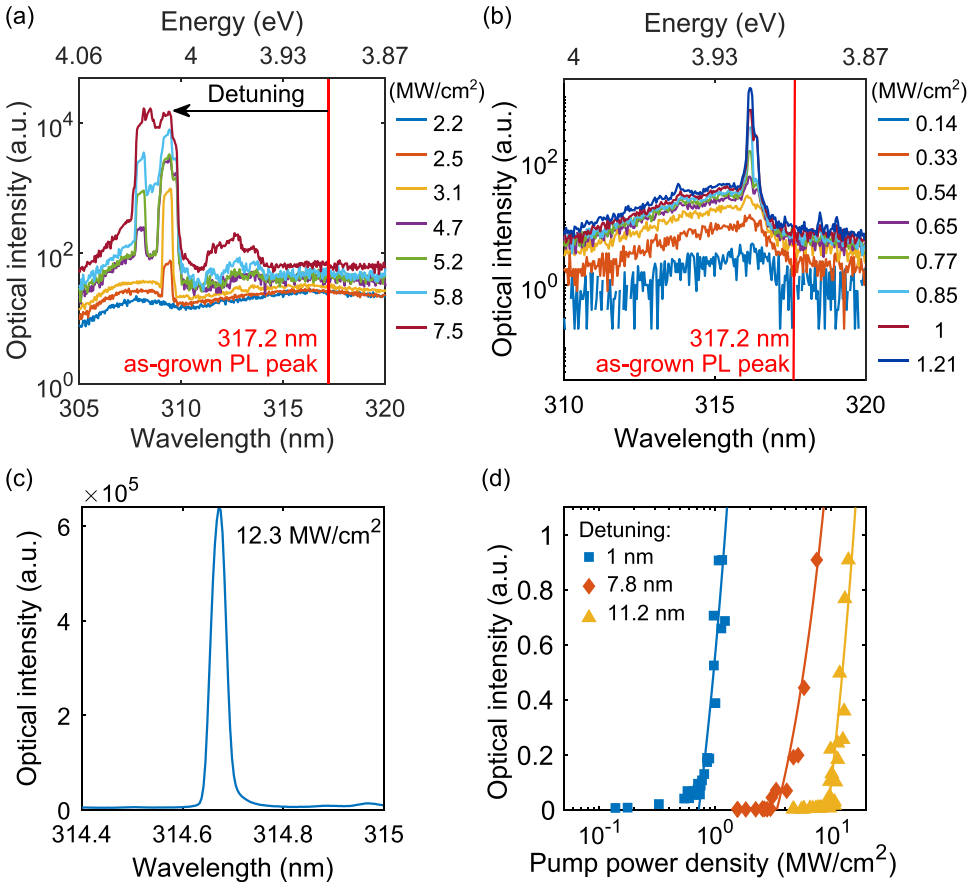

FIG. 4. Room-temperature photoluminescence spectra in logarithmic scale for increasing pump power density of (a) VCSELs B + 5 and (b) B + 13, with detuning of +7.8 and +1 nm, respectively (same VCSELs as in Fig. 3). The vertical red line indicates the as-grown PL peak of epitaxy B. (c) High-resolution PL spectrum of VCSEL B + 13 at 12.3 MW/cm^2. (d) Normalized optical emission intensity integrated over the dominant lasing peak as a function of the pump power density for VCSELs B0, B + 5, and B + 13 with the measured detuning of +11.2, +7.8, and +1 nm, respectively. The continuous lines indicate the linear fit above threshold.

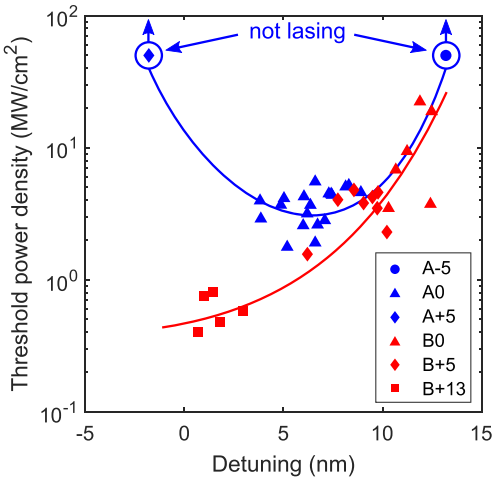

FIG. 5. Threshold power density as a function of the detuning, for VCSELs with cavity released by etching a bulk sacrificial layer (epitaxy A, blue) and a sacrificial multilayer (epitaxy B, red). The continuous lines are guides to the eye. The two circled points indicate VCSELs A−5 and A + 5 which did not lase up to pump power densities of 50 MW/cm^2.

using a sacrificial multilayer with similar detuning, due to the higher etched surface roughness in the former case. The VCSELs A + 5 showed no lasing but the resonance wavelength was measured around 320 nm, yielding a detuning of −1.8 nm. Compared to the VCSELs B + 13 grown with the sacrificial multilayer that exhibits the lowest threshold, the detuning is similar but the result is entirely different. For the VCSELs A + 5, the material gain at the spectral position of the resonance wavelength is too small to overcome the losses, due to the smaller joint density of states near the PL peak, and lasing could not be achieved. In this sample, the scattering losses are higher due to the increased roughness at the interface between the DBR and the cavity surface exposed by etching a bulk sacrificial layer [see Figs. 1(c) and 1(d)]. For the VCSELs A−5, lasing is not achieved for pump power densities up to 50 MW/cm^2, as the detuning is too large.

The comparison between VCSELs fabricated from different epitaxial structures is not straightforward as the VCSELs from epitaxy A with the bulk sacrificial layer have five QWs, while the VCSELs obtained from epitaxy B with the sacrificial multilayer have three QWs. Effective index method simulations predict a 26% lower threshold material gain in a five-QW sample compared to a three-QW sample, due to a higher optical confinement factor. Although the five-QW samples need a slightly higher pump power density to reach the same carrier density in the QWs and thereby the same blueshift of the gain spectrum as for the three-QW samples, the higher confinement factor in the five QWs should simultaneously provide higher modal gain when reaching that level. Thus, the different number of QWs could only account for relatively small threshold differences between the two samples. The significantly lower threshold observed for the VCSELs fabricated from sample B is believed to mainly originate from the reduced roughness of the surface after electrochemical etching of the sacrificial multilayer, resulting in lower optical scattering losses at the interface between cavity and top DBR and in the top DBR.

In conclusion, by optimizing the position of the resonance wavelength relative to the peak of the gain spectrum, a very low lasing threshold of 0.4 MW/cm^2 was achieved in UVB VCSELs with detuning smaller than 5 nm. This was only possible for samples with smoother cavity interfaces, i.e., an RMS roughness of 1.7 nm instead of 3.9 nm, allowing for lower threshold power densities and lasing in devices with a wider range of detunings. These results demonstrate the benefit of using electrochemical etching of AlGaN sacrificial layers for substrate removal and the deposition of dielectric cavity length adjustment layers on both sides of the cavity. The combination of these techniques will be of particular importance for electrically driven devices, where the access to both sides of the cavity allows the precise spatial alignment of the optical field intensity with loss and gain regions. Our results show the importance of smooth surfaces and accurate cavity length control for achieving low-threshold, high-performing UV VCSELs.

The authors thank Arne Knauer from Ferdinand-Braun-Institute for the development of the templates and Sylvia Hagedorn from Ferdinand-Braun-Institute for providing the AlN/sapphire. This work was performed in part at Myfab Chalmers, and the project was financially supported by the Swedish Research Council (No. 2018-00295), the European Research Council (ERC) under the European Union's Horizon 2020 research and innovation program (Grant Agreement No. 865622), the German Federal Ministry of Education and Research (BMBF) within the "Advanced UV for Life" consortium, and by the Deutsche Forschungsgemeinschaft (DFG) within the Collaborative Research Center "Semiconductor Nanophotonics (SFB 787)." The TEM images were taken as part of the DFG core facility project Berlin Electron Microscopy Network (Berlin EM Network).

AUTHOR DECLARATIONS

Conflict of Interest

The authors have no conflicts to disclose.

Author Contributions

Giulia Cardinali: Conceptualization (equal); Data curation (lead); Formal analysis (equal); Investigation (lead); Methodology (lead); Writing – original draft (lead); Writing – review & editing (lead). **Tim Kolbe:** Investigation (supporting); Methodology (supporting); Writing – review & editing (supporting). **Tim Wernicke:** Conceptualization (equal); Formal analysis (equal); Investigation (supporting); Methodology (supporting); Project administration (equal); Supervision (equal); Writing – review & editing (equal). **Åsa Haglund:** Conceptualization (equal); Formal analysis (equal); Funding acquisition (equal); Investigation (supporting); Methodology (supporting); Project administration (equal); Resources (equal); Supervision (equal); Writing – review & editing (equal). **Michael Kneissl:** Conceptualization (equal); Funding acquisition (equal); Project administration (equal); Supervision (equal); Writing – review & editing (equal). **Filip Hjort:** Conceptualization (equal); Data curation (supporting); Formal analysis (supporting); Investigation (equal); Methodology (equal); Writing – review & editing (supporting). **Nando Prokop:** Data curation (supporting); Investigation (supporting); Methodology (supporting); Writing – review & editing (supporting). **Johannes Enslin:** Investigation (supporting); Methodology (supporting); Writing – review & editing (supporting). **Munise Cobet:** Formal analysis (equal);

Investigation (equal); Methodology (equal); Supervision (supporting); Writing – review & editing (supporting). **Michael A. Bergmann:** Investigation (supporting); Methodology (supporting); Writing – review & editing (supporting). **Johan Gustavsson:** Investigation (supporting); Methodology (supporting); Software (equal); Writing – review & editing (supporting). **Joachim Ciers:** Formal analysis (equal); Investigation (supporting); Methodology (supporting); Writing – review & editing (supporting). **Ines Häusler:** Investigation (supporting); Methodology (supporting); Writing – review & editing (supporting).

DATA AVAILABILITY

The data that support the findings of this study are available from the corresponding author upon reasonable request.

REFERENCES

[1]R. Michalzik, *Fundamentals, Technology and Applications of Vertical-Cavity Surface-Emitting Lasers* (Springer, Berlin, Heidelberg, 2013).
[2]T. Mudigonda, T. S. Dabade, C. E. West, and S. R. Feldman, "Therapeutic modalities for localized psoriasis: 308-nm UVB excimer laser versus nontargeted phototherapy," Cutis **90**, 149–154 (2012); available at https://www.mdedge.com/dermatology/article/68463/psoriasis/therapeutic-modalities-localized-psoriasis-308-nm-uvb-excimer.
[3]S. Shin, S.-K. Hann, and S. H. Oh, "Combination treatment with excimer laser and narrowband UVB light in vitiligo patients," Photodermatol., Photoimmunol. Photomed. **32**, 28–33 (2016).
[4]S. Khan, D. Newport, and S. L. Calvé, "Gas detection using portable deep-UV absorption spectrophotometry: A review," Sensors **19**, 5210 (2019).
[5]J. Bennett, "Measuring UV curing parameters of commercial photopolymers used in additive manufacturing," Addit. Manuf. **18**, 203–212 (2017).
[6]A. Benjamin, R. Abbasi, M. Owens, R. Olsen, D. Walsh, T. LeFevre, and J. Wilking, "Light-based 3D printing of hydrogels with high-resolution channels," Biomed. Phys. Eng. Express **5**, 025035 (2019).
[7]M. A. Würtele, T. Kolbe, M. Lipsz, A. Külberg, M. Weyers, M. Kneissl, and M. Jekel, "Application of GaN-based ultraviolet-C light emitting diodes-UV LEDs-for water disinfection," Water Res. **45**, 1481–1489 (2011).
[8]M. A. Banas, M. H. Crawford, D. S. Ruby, M. P. Ross, J. S. Nelson, "A. A. Allerman, and R. Boucher, "Final LDRD report: Ultraviolet water purification systems for rural environments and mobile applications," Technical Report No. SAND2005-7245 (Sandia National Laboratories, Albuquerque, NM, 2005).
[9]D.-K. Kim, D.-H. Kang, and J. L. Schottel, "UVC LED irradiation effectively inactivates aerosolized viruses, bacteria, and fungi in a chamber-type air disinfection system," Appl. Environ. Microbiol. **84**, e00944-18 (2018).
[10]F. Hjort, J. Enslin, M. Cobet, M. A. Bergmann, J. Gustavsson, T. Kolbe, A. Knauer, F. Nippert, I. Häusler, M. R. Wagner, T. Wernicke, M. Kneissl, and Å. Haglund, "A 310 nm optically pumped AlGaN vertical-cavity surface-emitting laser," ACS Photonics **8**, 135–141 (2021).
[11]Z. Zheng, Y. Mei, H. Long, J. Hoo, S. Guo, Q. Li, L. Ying, Z. Zheng, and B. Zhang, "AlGaN-based deep ultraviolet vertical-cavity surface-emitting laser," IEEE Electron Device Lett. **42**, 375–378 (2021).
[12]H. Amano, R. Collazo, C. D. Santi, S. Einfeldt, M. Funato, J. Glaab, S. Hagedorn, A. Hirano, H. Hirayama, R. Ishii, Y. Kashima, Y. Kawakami, R. Kirste, M. Kneissl, R. Martin, F. Mehnke, M. Meneghini, A. Ougazzaden, P. J. Parbrook, S. Rajan, P. Reddy, F. Römer, J. Ruschel, B. Sarkar, F. Scholz, L. J. Schowalter, P. Shields, Z. Sitar, L. Sulmoni, T. Wang, T. Wernicke, M. Weyers, B. Witzigmann, Y.-R. Wu, T. Wunderer, and Y. Zhang, "The 2020 UV emitter roadmap," J. Phys. D **53**, 503001 (2020).
[13]T.-C. Chang, S.-Y. Kuo, J.-T. Lian, K.-B. Hong, S.-C. Wang, and T.-C. Lu, "High-temperature operation of GaN-based vertical-cavity surface-emitting lasers," Appl. Phys. Express **10**, 112101 (2017).
[14]T.-C. Lu, T.-T. Wu, S.-W. Chen, P.-M. Tu, Z.-Y. Li, C.-K. Chen, C.-H. Chen, H.-C. Kuo, S.-C. Wang, H.-W. Zan, and C.-Y. Chang, "Characteristics of current-injected GaN-based vertical-cavity surface-emitting lasers," IEEE J. Sel. Top. Quantum Electron. **17**, 1594–1602 (2011).
[15]C. O. Holder, J. T. Leonard, R. M. Farrell, D. A. Cohen, B. Yonkee, J. S. Speck, S. P. DenBaars, S. Nakamura, and D. F. Feezell, "Nonpolar III-nitride vertical-cavity surface emitting lasers with a polarization ratio of 100% fabricated using photoelectrochemical etching," Appl. Phys. Lett. **105**, 031111 (2014).
[16]W. W. Chow, A. Girndt, and S. W. Koch, "Calculation of quantum well laser gain spectra," Opt. Express **2**, 119–124 (1998).
[17]W. W. Chow and M. Kneissl, "Laser gain properties of AlGaN quantum wells," J. Appl. Phys. **98**, 114502 (2005).
[18]C. Chen, P. O. Leisher, A. A. Allerman, K. M. Geib, and K. D. Choquette, "Temperature analysis of threshold current in infrared vertical-cavity surface-emitting lasers," IEEE J. Quantum Electron. **42**, 1078–1083 (2006).
[19]M. Kuramoto, S. Kobayashi, T. Akagi, K. Tazawa, K. Tanaka, K. Nakata, and T. Saito, "Watt-class blue vertical-cavity surface-emitting laser array," Appl. Phys. Express **12**, 091004 (2019).
[20]R. T. Elafandy, J.-H. Kang, B. Li, T. K. Kim, J. S. Kwak, and J. Han, "Room-temperature operation of c-plane GaN vertical cavity surface emitting laser on conductive nanoporous distributed Bragg reflector," Appl. Phys. Lett. **117**, 011101 (2020).
[21]S. Mishkat-Ul-Masabih, A. Aragon, M. Monavarian, T. Luk, and D. Feezell, "Electrically injected nonpolar GaN-based VCSELs with lattice-matched nanoporous distributed Bragg reflector mirrors," Appl. Phys. Express **12**, 036504 (2019).
[22]J. A. Kearns, J. Back, D. A. Cohen, S. P. DenBaars, and S. Nakamura, "Demonstration of blue semipolar (20 $\bar{2}$1) GaN-based vertical-cavity surface-emitting lasers," Opt. Express **27**, 23707–23713 (2019).
[23]K. Terao, H. Nagai, D. Morita, S. Masui, T. Yanamoto, and S. Nagahama, "Blue and green GaN-based vertical-cavity surface-emitting lasers with AlInN/GaN DBR," Proc. SPIE **11686**, 116860E (2021).
[24]R. B. Xu, Y. Mei, B. P. Zhang, L. Y. Ying, Z. W. Zheng, W. Hofmann, J. P. Liu, H. Yang, M. Li, and J. Zhang, "Simultaneous blue and green lasing of GaN-based vertical-cavity surface-emitting lasers," Semicond. Sci. Technol. **32**, 105012 (2017).
[25]S. Lee, C. Forman, C. Lee, J. Kearns, E. Young, J. Leonard, D. Cohen, J. Speck, S. Nakamura, and S. Denbaars, "GaN-based vertical-cavity surface-emitting lasers with tunnel junction contacts grown by metal-organic chemical vapor deposition," Appl. Phys. Express **11**, 062703 (2018).
[26]S. Lee, C. A. Forman, J. Kearns, J. T. Leonard, D. A. Cohen, S. Nakamura, and S. P. DenBaars, "Demonstration of GaN-based vertical-cavity surface-emitting lasers with buried tunnel junction contacts," Opt. Express **27**, 31621–31628 (2019).
[27]K. Kiyohara, M. Odawara, T. Takeuchi, S. Kamiyama, M. Iwaya, I. Akasaki, and T. Saito, "Room-temperature continuous-wave operations of GaN-based vertical-cavity surface-emitting lasers with buried GaInN tunnel junctions," Appl. Phys. Express **13**, 111003 (2020).
[28]W. Liu, X.-L. Hu, L. Ying, J.-Y. Zhang, and B.-P. Zhang, "Room temperature continuous wave lasing of electrically injected GaN-based vertical cavity surface emitting lasers," Appl. Phys. Lett. **104**, 251116 (2014).
[29]T. Hamaguchi, M. Tanaka, and H. Nakajima, "A review on the latest progress of visible GaN-based VCSELs with lateral confinement by curved dielectric DBR reflector and boron ion implantation," Jpn. J. Appl. Phys. **58**, SC0806 (2019).
[30]T. Onishi, O. Imafuji, K. Nagamatsu, M. Kawaguchi, K. Yamanaka, and S. Takigawa, "Continuous wave operation of GaN vertical cavity surface emitting lasers at room temperature," IEEE J. Quantum Electron. **48**, 1107–1112 (2012).
[31]Z. Zheng, Y. Li, O. Paul, H. Long, S. Matta, M. Leroux, J. Brault, L. Ying, Z. Zheng, and B. Zhang, "Loss analysis in nitride deep ultraviolet planar cavity," J. Nanophotonics **12**, 1–8 (2018).
[32]Z. Zheng, H. Long, S. Matta, M. Leroux, J. Brault, L. Ying, Z. Zheng, and B. Zhang, "Photoassisted chemical smoothing of AlGaN surface after laser lift-off," J. Vac. Sci. Technol. B **38**, 042207 (2020).
[33]H. K. Cho, O. Krüeger, A. Külberg, J. Rass, U. Zeimer, T. Kolbe, A. Knauer, S. Einfeldt, M. Weyers, and M. Kneissl, "Chip design for thin-film deep ultraviolet LEDs fabricated by laser lift-off of the sapphire substrate," Semicond. Sci. Technol. **32**, 12LT01 (2017).
[34]C. Holder, J. S. Speck, S. P. DenBaars, S. Nakamura, and D. Feezell, "Demonstration of nonpolar GaN-based vertical-cavity surface-emitting lasers," Appl. Phys. Express **5**, 092104 (2012).
[35]A. R. Stonas, T. Margalith, S. P. DenBaars, L. A. Coldren, and E. L. Hu, "Development of selective lateral photoelectrochemical etching of InGaN/GaN for lift-off applications," Appl. Phys. Lett. **78**, 1945–1947 (2001).

[36]M. A. Bergmann, J. Enslin, R. Yapparov, F. Hjort, B. Wickman, S. Marcinkevičius, T. Wernicke, M. Kneissl, and Å. Haglund, "Electrochemical etching of AlGaN for the realization of thin-film devices," Appl. Phys. Lett. **115**, 182103 (2019).
[37]M. A. Bergmann, J. Enslin, F. Hjort, T. Wernicke, M. Kneissl, and Å. Haglund, "Thin-film flip-chip UVB LEDs realized by electrochemical etching," Appl. Phys. Lett. **116**, 121101 (2020).
[38]J. Enslin, F. Mehnke, A. Mogilatenko, K. Bellmann, M. Guttmann, C. Kuhn, J. Rass, N. Lobo-Ploch, T. Wernicke, M. Weyers, and M. Kneissl, "Metamorphic $Al_{0.5}Ga_{0.5}N$:Si on AlN/sapphire for the growth of UVB LEDs," in *Proceedings of the 18th International Conference on Metal Organic Vapor Phase Epitaxy, 2017* [J. Cryst. Growth **464**, 185–189 (2017)].
[39]J. Ciers, M. A. Bergmann, F. Hjort, J.-F. Carlin, N. Grandjean, and Å. Haglund, "Smooth GaN membranes by polarization-assisted electrochemical etching," Appl. Phys. Lett. **118**, 062107 (2021).
[40]A. B. Vasista, D. K. Sharma, and G. V. P. Kumar, "Fourier plane optical microscopy and spectroscopy," in *Digital Encyclopedia of Applied Physics* (American Cancer Society, 2019) pp. 1–14.
[41]M. S. Skolnick, T. A. Fisher, and D. M. Whittaker, "Strong coupling phenomena in quantum microcavity structures," Semicond. Sci. Technol. **13**, 645–669 (1998).
[42]G. R. Hadley, "Effective index model for vertical-cavity surface-emitting lasers," Opt. Lett. **20**, 1483–1485 (1995).
[43]J. T. Leonard, D. A. Cohen, B. P. Yonkee, R. M. Farrell, T. Margalith, S. Lee, S. P. DenBaars, J. S. Speck, and S. Nakamura, "Nonpolar III-nitride vertical-cavity surface-emitting lasers incorporating an ion implanted aperture," Appl. Phys. Lett. **107**, 011102 (2015).
[44]S. Wang, T. Lu, C. Kao, J. T. Chu, G. Huang, H. Kuo, S. Chen, T. Kao, J. Chen, and L.-F. Lin, "Optically pumped GaN-based vertical cavity surface emitting lasers: Technology and characteristics," Jpn. J. Appl. Phys. **46**, 5397–5407 (2007).